Biophysical Chemistry, 43 (1992) 9–19
Elsevier Science Publishers B.V., Amsterdam

BIOCHE 01645

Computer simulation of the structure of DNA molecules in an electric field

Christer Elvingson

Department of Physical Chemistry, Chalmers University of Technology, S-412 96 Göteborg (Sweden)

(Received 15 July 1991; accepted in revised form 11 October 1991)

Abstract

The structure of a model DNA chain in an electric field is investigated by Brownian dynamics simulations. The molecules have been modelled as discrete wormlike chains consisting of charged spherical subunits. The effects of hydrodynamic interactions and counterion polarization have been studied separately. Including only the polarization of the counterions causes the polyelectrolyte chain to orient in the form of a stiff rod. Taking also the hydrodynamic interactions into account, however, has the effect of deforming the chain during orientation into a bent configuration which results in a decrease of the orientational time constant. Furthermore, even without polarization effects, the hydrodynamics alone can cause an orientation of the chain, although at a lower level.

Keywords: Hydrodynamics; Electric dichroism; Brownian dynamics simulation; Dipole moment; Polyelectrolytes; Orientation mechanism

1. Introduction

The rotational and intramolecular dynamics of biological macromolecules in solution is the subject of continuous study [1,2]. Double helical DNA especially has been much studied [3–5], because the structure and flexibility of DNA are important properties in its biological function as expressed e.g. in replication and packing processes [6,7]. Both theory and experiments on DNA and other semiflexible molecules, however, pose considerable difficulties, particularly if one wishes to calculate dynamical properties such as rotational time correlation functions. Some of the models which have been used, like the Rouse–Zimm model [8], have not included the stiffness of the molecules, while other theories have been using a free draining wormlike chain model [9]. One way to include the relative rigidity of a wormlike chain and also account for the hydrodynamic coupling between different parts of the molecule is to use Brownian dynamics simulation [10]. This method has recently been used for studying the dynamic light scattering and fluorescence depolarization of chains at equilibrium [11,12]. A more critical test of the interplay between a molecule's structure and its dynamics is to try to calculate properties obtained by electro-optical measurements such as transient electric birefringence or electric dichroism where molecules are oriented by applying electric field pulses [1,13,14]. Such measurements are often used to determine rota-

Correspondence to: Dr. C. Elvingson, Department of Physical Chemistry, Chalmers University of Tecynology, S-412 96 Göteborg (Sweden).

tional correlation times and thus to estimate the dimensions of the corresponding biopolymer molecules [15], since the decay of the electric birefringence or dichroism is very sensitive to the size of the molecule or the changes of the molecule's shape.

When interpreting such experiments on DNA, the molecule is usually assumed to orient like a dipole in the form of a stiff rod. For short chains or low electric field strengths, the orientation seems to be accurately described by an induced dipole mechanism, while for longer DNA fragments or higher electric fields, an increased deviation from the induced dipole mechanism prediction is observed [4]. Analysis of the data for the high field case suggests the existence of a large permanent dipole moment, in spite of the fact that B-DNA is an anti-parallel double helix and should have no permanent dipole moment. This permanent contribution has been attributed either to a saturation of the field dependent polarization of the counterion atmosphere along a rigid rod [16], or to the DNA having a highly bent *equilibrium* structure [17,18]. For a charged molecule such as DNA, a permanent dipole has physical meaning only with respect to the centre of hydrodynamic resistance or diffusion and this would give a permanent dipole moment for a DNA molecule in the form of e.g. a circular arc. It has also been proposed that the permanent dipole moment contribution could be due to the asymmetric binding of charged ligands to the DNA [19]. The deviation from an induced dipole mechanism seems, however, to persist also in experiments in pure buffer solution [20]. The decay curves in dichroism or birefringence experiments also show that the amplitude of the faster of the two relaxation processes usually seen, increases significantly when the electric field strength increases. This has been attributed to either a straightening of the chain from a highly bent equilibrium structure [17], to two different time constants for the counter ion polarization [3], to the exchange of energy between different modes [3] or, recently, to a bending of the chain when the field strength is increasing [21]. One has not, however, been able to envisage a reason for the last mechanism.

All the dynamical simulations performed so far have tried to investigate the off-field relaxation by simulating the dynamics of chains at equilibrium [11,12,22]. It is, however, reasonable to believe that the electric field should have some influence on the properties of the chain during the orientation. One would thus endeavour to simulate the motion of a polyelectrolyte chain both during the orientation and decay processes of an electro-optical experiment. Since the orientational motion of the molecule is a dynamical process, it should be important to include not only the inherent flexibility of DNA but also the hydrodynamic coupling between different parts of the molecule. Hydrodynamic interactions have been shown to be of importance in e.g. simulations of coagulation processes where the final aggregate structure depended upon whether the hydrodynamic interactions were included or not [23]. To that end, a number of simulations have been performed to investigate what happens to a biopolymer molecule when it orients in an electric field.

The outline of this paper is as follows. In section two the chain model and the dynamics algorithm are outlined together with a definition of the properties used when analyzing the shape characteristics and orientation of the molecules. In the third section, the results of the simulations are presented, while the paper ends with a discussion of these results.

2. Computational details

In the present study, a discrete wormlike chain model is used [11,24,25] consisting of 20 charged spherical subunits of radius a equal to 1.59 nm linked by harmonic forces with $\langle r_{i,i+1} - 2a \rangle = 0$ and $\langle (r_{i,i+1} - 2a)^2 \rangle = a^2/25$, where $r_{i,i+1}$ is the distance between subunits i and $i+1$. The electrostatic interactions between the different segments are not explicitly included but the resulting stiffness of the chain is invoked by a quadratic bending potential [11,24] with a bending force constant chosen to mimic a persistence length of 30 nm. This persistence length, being in the lower range of that usually used, was chosen because

we wanted to study the effect of chain flexibility on the orientational properties. The hydrodynamic interactions between the subunits were calculated using the Rotne–Prager diffusion tensor [26] which for $i = j$ is given by

$$\mathbf{D}_{ii} = \frac{kT}{6\pi\eta a}\mathbf{I} \tag{1a}$$

and for different but non-overlapping subunits by

$$\mathbf{D}_{ij} = \frac{kT}{8\pi\eta r_{ij}}\left[\mathbf{I} + \hat{\boldsymbol{r}}_{ij}\hat{\boldsymbol{r}}_{ij} + \frac{2a^2}{r_{ij}^2}\left(\frac{1}{3}\mathbf{I} - \hat{\boldsymbol{r}}_{ij}\hat{\boldsymbol{r}}_{ij}\right)\right] \tag{1b}$$

while for overlapping beads, the corresponding expression is

$$\mathbf{D}_{ij} = \frac{kT}{6\pi\eta a}\left[\left(1 - \frac{9r_{ij}}{32a}\right)\mathbf{I} + \frac{3\mathbf{r}_{ij}\mathbf{r}_{ij}}{32ar_{ij}}\right] \tag{1c}$$

where $\boldsymbol{r}_{ij} = \boldsymbol{r}_j - \boldsymbol{r}_i$, $r_{ij} = |\boldsymbol{r}_{ij}|$, and a 'hat' denotes a unit vector, $\mathbf{I}$ is the unit tensor, η is the viscosity, T is the temperature, and k is the Boltzmann constant. The starting configurations were sampled from an equilibrium ensemble and the direction of the electric field chosen at random for each trajectory. The dynamics of the polyelectrolyte chain was simulated using a Brownian dynamics algorithm, where the change in position of subunit i during a time step Δt is given by [10]

$$\Delta\boldsymbol{r}_i = \frac{\Delta t}{kT}\sum_{j=1}^{N}\mathbf{D}_{ij}^0\cdot\mathbf{F}_j^0 + \Delta t\sum_{j=1}^{N}\nabla_j\cdot\mathbf{D}_{ij}^0 + \mathbf{R}_i\left(\mathbf{D}_{ij}^0, \Delta t\right). \tag{2}$$

where $\mathbf{F}_j$ is the direct force on subunit j, and $\boldsymbol{R}_i$ is a vector of Gaussian random numbers with zero mean and $\langle \boldsymbol{R}_i\boldsymbol{R}_j\rangle = 2\mathbf{D}_{ij}\Delta t$, while a zero superscript denotes the value at the beginning of a time step. In the present simulations $T = 278$ K, $\Delta t = 0.1$ ns, and the charge of each subunit was set equal to $5q_e$, where q_e is the elementary charge. This charge has either been fixed on the subunits or has been distributed along the chain according to a procedure described below. Using the Rotne–Prager diffusion tensor has the advantage that it is positive definite for all inter-subunit distances and that is has a zero divergence. If a variational approach is used when deriving the diffusion tensor (as for the Rotne–Prager tensor), one can also define an expression for the hydrodynamic interaction in cases when the beads might overlap (eq. 1c), by regarding overlapping spheres as truncated non-overlapping spheres and thus making it possible to handle a fuller range of molecular geometries. The Rotne–Prager tensor also compares favourably with calculations of the translational diffusion coefficient using multiparticle hydrodynamic interactions, where the higher powers of R^{-1} seem to cancel each other [27].

The stochastic displacement vectors are obtained by writing $\boldsymbol{R} = \boldsymbol{\sigma}\cdot\boldsymbol{X}$, where $\boldsymbol{X}$ is a vector of Gaussian random numbers with $\langle \boldsymbol{X}_i\rangle = 0$ and $\langle \boldsymbol{X}_i\boldsymbol{X}_j\rangle = 2\Delta t\delta_{ij}$, and $\boldsymbol{\sigma}$ is obtained from $\mathbf{D} = \boldsymbol{\sigma}\boldsymbol{\sigma}^{\mathrm{T}}$, where $\boldsymbol{\sigma}^{\mathrm{T}}$ is the transpose. Since $\mathbf{D}$ in this case is symmetric, $\boldsymbol{\sigma}$ is usually obtained using a Cholesky factorization [28]. As an N^3 operation, however, this limits the number of subunits that can be treated when the diffusion tensor is updated every time step, even though the corresponding calculations can be efficiently vectorized [29]. For chains at equilibrium, preaveraged hydrodynamic interactions are often used, which seems to give good results for these cases [11]. In the present simulations, though, we have a non-equilibrium situation, where the chains in some cases are far from their equilibrium shape and we thus want to recalculate the configuration dependent diffusion tensor and the corresponding "square root", $\boldsymbol{\sigma}$, during the course of a simulation. An alternative way to obtain $\boldsymbol{\sigma}$ is to use a Chebyshev polynomial expansion [30] and this method is also faster than the Cholesky factorization [29]. The order of the polynomial required for a certain maximum error depends on the ratio between the largest and smallest eigenvalues of $\mathbf{D}$, and we have in the present paper used an eighth order polynomial which should give the correct result within one per cent even when the difference between the extreme eigenvalues of $\mathbf{D}$ increases to a factor of 50 [30]. The change in the shape of the molecules in some of the simulations has been quite large, however, and the coefficients in the Chebyshev expansion have also been recalculated at regular intervals during each trajectory.

Since we are interested in polyelectrolyte molecules, one has also to take into account the polarization of the counterion atmosphere in the electric field. In the present simulation, this effect has been included in some of the trajectories by redistributing the charge of the subunits in the following way [29]: For each substring of consecutive beads for which the scalar product between the electric field and the bond vectors has the same sign, the charge is distributed over the bonds proportional to $1/\sqrt{N_i}$, where N_i is the order of the bead in the substring.

The trajectories have been analyzed with respect to the structure of the chains both during the process of orientation and also during the relaxation back to equilibrium after the electric field has been turned off, and ensemble averages over 100 trajectories have been used when calculating the time dependencies shown in the next section. The error bars on certain data points in the figures show the corresponding standard deviations. Besides determining the end-to-end distance, R_{ee}, the shape of the molecules as expressed in the degree of oblateness/prolateness, S, has also been calculated, where S is defined by [31]

$$S = \frac{27\left\langle \prod_{i=1}^{3} (\lambda_i - \bar{\lambda}) \right\rangle}{\left\langle \left(\sum_{i=1}^{3} \lambda_i \right)^3 \right\rangle} \tag{3}$$

where the lambdas are the eigenvalues of the components of the radius of gyration tensor, $\bar{\lambda}$ being the average eigenvalue.

The dipole moments of the molecules were also calculated starting from the standard equation

$$\boldsymbol{\mu} = \sum_{i=1}^{N} q_i \boldsymbol{r}_i \tag{4}$$

where q_i is the charge of subunit i. In the case of a charged molecule like DNA, however, the dipole moment is dependent upon the choice of origin and the permanent dipole moment has been calculated referring to the centre of diffusion of the molecule. This is the point for which the translation–rotation coupling diffusion tensor is symmetric [32]. The centre of diffusion was calculated according to the procedure by García de la Torre et al. [33,34] where the distance vector from the origin to the centre of diffusion, $\boldsymbol{r}_D$, is given by

$$\boldsymbol{r}_D = \begin{pmatrix} D_r^{22} + D_r^{33} & -D_r^{12} & -D_r^{13} \\ -D_r^{12} & D_r^{11} + D_r^{33} & -D_r^{23} \\ -D_r^{13} & -D_r^{23} & D_r^{11} + D_r^{22} \end{pmatrix}^{-1} \times \begin{pmatrix} D_c^{23} - D_c^{32} \\ D_c^{31} - D_c^{13} \\ D_c^{12} - D_c^{21} \end{pmatrix} \tag{5}$$

where $\mathbf{D}_r$ is the rotational diffusion tensor and $\mathbf{D}_c$ the translation–rotation diffusion tensor. To emphasize the structure dependence of the calculated dipole moments for a charged molecule, all dipole moments shown in the next section have been calculated according to $\mu \propto |\sum_{i=1}^{N}(\boldsymbol{r}_i - \boldsymbol{r}_D)|$, regardless of whether polarization effects were included in the "moving-on" algorithm or not.

To see how the structural changes calculated according to the procedures above will influence the orientation of the molecules, which is the quantity detected during dichroism or birefringence experiments, we have also calculated an orientation function $\mathscr{L}$ defined by

$$\mathscr{L}(t) = \frac{1}{N-1} \sum_{i=1}^{N-1} \left[\cos^2 \vartheta_{z_i}(t) - \frac{1}{2}\left(\cos^2 \vartheta_{x_i}(t) + \cos^2 \vartheta_{y_i}(t) \right) \right] \tag{6}$$

where the z-axis is the direction of the electric field and ϑ_{z_i} is the angle between bond i and the z-axis. This definition of $\mathscr{L}$ thus results in zero for a random distribution and one for a perfectly aligned molecule.

3. Results

In Fig. 1 the end-to-end distance as a function of time is shown for different electric field strengths assuming fixed charges on the subunits.

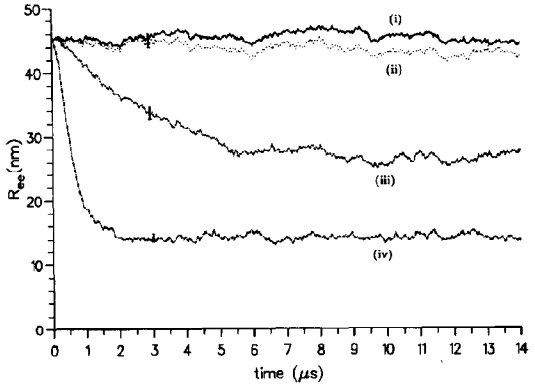

Fig. 1. End-to-end distance as a function of time for different electric field strengths: (i) $E = 4\ 10^6$ Vm^{-1}; (ii) $E = 2.5\ 10^5$ Vm^{-1}, (iii) $E = 1\ 10^6$ Vm^{-1}, (iv) $E = 4\ 10^6$ Vm^{-1}. In (i) without and in (ii)–(iv) with hydrodynamic interactions. Polarization effects not included.

First one can notice that the average end-to-end distance for the starting configurations is in agreement with the equilibrium value of 45.4 nm that can be obtained from the following relation for a continuous wormlike chain [35]

$$\langle R_{ee}^2 \rangle = 2LP\left[1 - P/L + (P/L)e^{-L/P}\right] \qquad (7)$$

where L is the contour length and P is the persistence length. Without any hydrodynamic coupling, the chains only translate without any significant change in their shape even for the highest field strength as shown for curve (i). Including the hydrodynamic interactions, though, considerably changes the picture. The end-to-end distance starts to decrease when the field is applied and the decrease is larger when the field strength is increased. For the highest field strength, the end-to-end distance rapidly drops to even less than half its starting value.

The chains are thus seen to be highly deformed from their equilibrium structure when increasing the electric field. Further insight about the global change in configuration can be obtained from the degree of oblateness/prolateness S of the chains. The limits for S are $-0.25 \leq S \leq 2$, and the sign of S determines whether the chains are predominantly oblate (negative) or prolate (positive) [31]. Curves (i) and (ii) in Fig. 2(a) show the time dependence of S, when the electric field is applied, for the same field strengths as for curves (iii) and (iv) in Fig. 1, whereas Fig. 2(b) shows the relaxation of S back to equilibrium after the field has been turned off. When applying the field, S decreases monotonically and the deviation from the molecules' original prolate equilibrium structure can become quite large as seen for curve (ii).

Another important property for understanding the structure and dynamics of polyelectrolyte molecules is the dipole moment, and in Fig. 3(a), the dipole moment with respect to the centre of diffusion is shown for the highest field strength. It is seen for curve (i) that with fixed charges, μ rapidly goes through a sharp maximum before it returns to a level close to the equilibrium value.

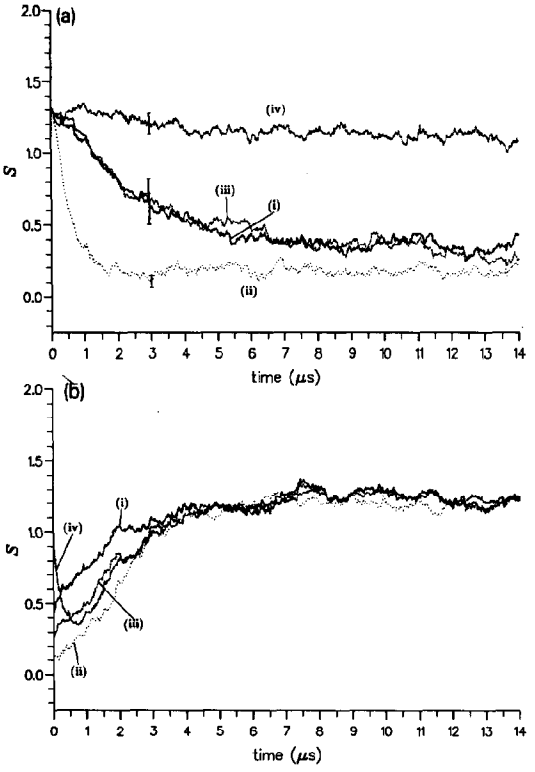

Fig. 2. (a) The degree of oblateness/prolateness, S, as a function of time for different electric field strengths: (i) $E = 1\ 10^6$ Vm^{-1}; (ii) $E = 4\ 10^6$ Vm^{-1}; (iii) $E = 1\ 10^6$ Vm^{-1}; (iv) $E = 4\ 10^6$ Vm^{-1}. In curves (iii)–(iv) polarization effects are included. (b) As in 2(a), but after the electric field has been turned off.

Figure 3(b) then shows that the relaxation back to equilibrium also proceeds through a maximum although this is smaller and the time for reaching equilibrium is larger than for reaching the steady-state in Fig. 3(a).

So far we have only considered the effect of the hydrodynamic interactions on the shape of the biopolymer molecules. The influence on the end-to-end distance of also including the counterion polarization, using the model discussed in the previous section, is seen Fig. 4. First we observe that without any hydrodynamic coupling, R_{ee} shows an initial increase when polarization effects are included. This effect is even more pronounced for the radius of gyration, R_g, (not shown) for which the relative straightening of the chain results in a distinctly larger value of R_g for

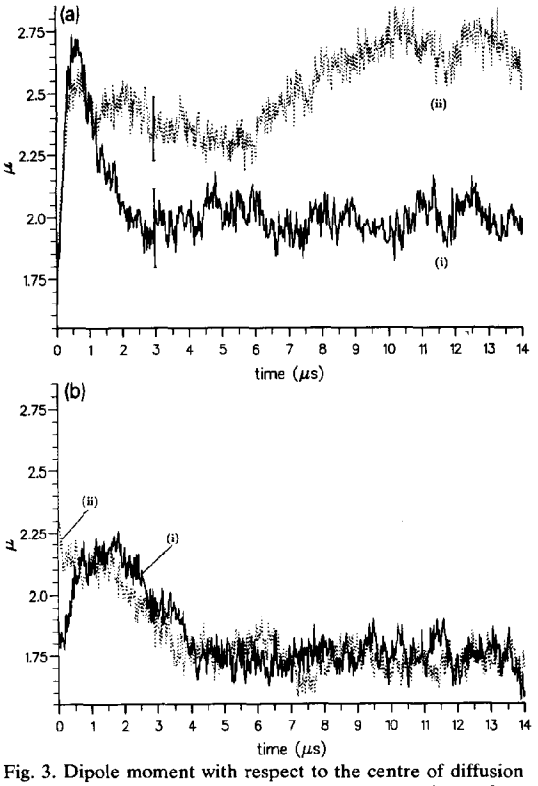

Fig. 3. Dipole moment with respect to the centre of diffusion in arbitrary units as a function of time for $E = 4\ 10^6\ Vm^{-1}$, in (i) without and in (ii) with polarization effects included. In both cases hydrodynamic interactions have been included. (b) As in 3(a), but after the electric field has been turned off.

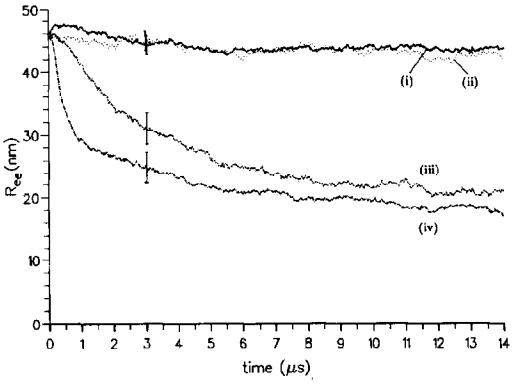

Fig. 4. As in Fig. 1, but with polarization effects included.

curve (i) compared to curve (ii) during the entire course of the simulation. This observation is in line with a model regarding the molecule as a wormlike chain which stiffens to a more rod-like shape under the influence of the orienting dipole forces originating from the polarization of the counterions [17]. Including the hydrodynamics and comparing curves (ii)–(iv) in Figs. 1 and 4 shows, however, that the molecule still becomes deformed due to the hydrodynamic interactions. The resulting average shape of the molecules has, however, changed when including polarization and although the end-to-end distance still decreases substantially, the large difference between curves (iii) and (iv) in Fig. 1 is reduced in Fig. 4.

The importance of including both the polarization effects and the hydrodynamic interactions with respect to the global change of the molecules' shape is also reflected in the change in S shown in Fig. 2(a). Comparing curves (ii) and (iv) shows that, when the molecules are not experiencing any polarization forces, the decrease in S is quite large, as noted above, but including polarization counteracts this tendency of the molecule becoming increasingly oblate and S remains at a relatively high value during the entire electric pulse. The difference is even more pronounced when comparing what happens during the return to equilibrium after the field has been turned off, shown in Fig. 2(b). While all other curves increase continuously, S goes through a minimum for curve (iv), when returning to equilibrium. This

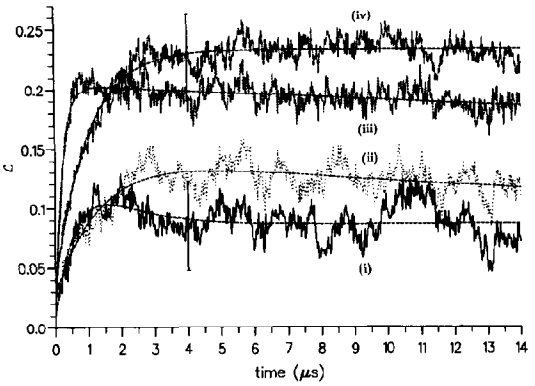

Fig. 5. Orientation, $\mathscr{L}$, as a function of time for (i), (iii)–(iv) $E = 4\ 10^6\ \mathrm{Vm}^{-1}$ and (ii) $E = 1\ 10^6\ \mathrm{Vm}^{-1}$. In (i) only hydrodynamic interactions are included and in (ii)–(iii) both hydrodynamic interactions and polarization effects are taken into account, while in (iv) only the polarization effects are included. For curves (i)–(iii), the results of a two exponential fit are shown while a single-exponential fit is indicated for curve (iv).

difference when including polarization is also clearly seen in Fig. 3. The dipole moment when including polarization also shows a rapid increase when the field is turned on. It does not, however, go through a maximum which is the case when only the hydrodynamic coupling is included, but continues to stay at a high level during the entire pulse.

The structural changes dealt with so far when the electric field is switched on or off are not so easily observed experimentally. What is usually measured is the orientation as expressed by the dichroism or birefringence. To see how the changes in shape, described above, affect the orientational properties of the polyelectrolyte molecules, $\mathscr{L}$ as a function of time is shown in Fig. 5. These curves are somewhat more noisy than the curves in previous figures, since the spread of the initial orientation of the chains with respect to the electric field is larger than compared to an intrinsic property like the end-to-end distance. We can first observe that even without any polarization effects, one gets a hydrodynamically induced orientation of the chain, shown by curve (i). The degree of orientation, however, is in this case not very large since we do not have any 'direct' orienting forces, but the orientation is merely a result of the different mobilities of the subunits as a function of the chain configuration, to be discussed below. The result of also including the polarization shows that the steady-state orientation develops faster and the amplitude is larger in this case. This can e.g. be seen from curve (ii) in Fig. 5 showing the orientation at a smaller field strength than for curve (i), but still giving a somewhat larger orientation, when the orienting dipolar forces are included. We then look at curves (iii) and (iv) showing the orientation at the highest field with and without hydrodynamic interactions. These curves are quite similar, in spite of the difference between the structural characteristics as evidenced by the results shown above. The main difference being that orienting the molecule in the form of a stiff rod, curve (iv), is a slower process than compared to a contemporaneous orientation and bending of the molecule, reducing its largest dimension, curve (iii). Although the curves, when including hydrodynamic coupling, are somewhat too noisy to allow the definite determination of time constants, the best fit is obtained by using a sum of two exponentials, since curves (i)–(iii) all exhibit a small but distinct overshoot before reaching a steady-state. This is in contrast to curve (iv) which represents an orientation without any decrease of the end-to-end vector and where a single-exponential fit well describes the orientation process as seen Fig. 5.

4. Discussion

To understand the mechanisms behind the structural changes during electric field orientation presented in the previous section, we start by looking at some simple model calculations. Assume we begin with the chain placed along the x-axis, and apply a field in the z-direction. Using eq. (2) but "switching off" the Brownian motion for clarity, during a time step Δt the displacement Δz for the subunits in the middle will be larger than for the beads at the ends, and this difference will be larger when increasing the field. This effect is illustrated in Fig. 6, which shows the configurations after 2 μs for the same field

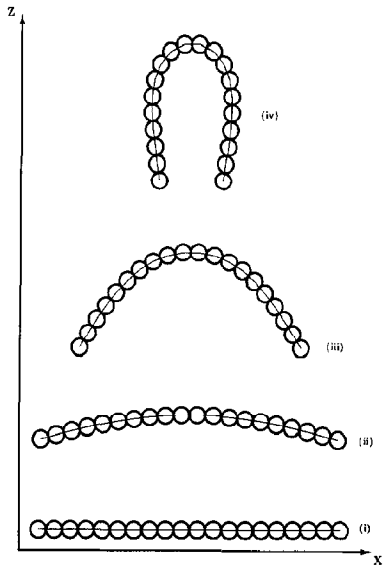

Fig. 6. Chain configurations after 2 μs starting from chains parallel with the x-axis and applying a field in the z-direction. The distances between the different configurations are arbitrary and have been chosen for ease of inspection. The details of the calculations are given in the text. (i) $E = 4\ 10^6$ Vm^{-1}; (ii) $E = 2.5\ 10^5$ Vm^{-1}; (iii) $E = 1\ 10^6$ Vm^{-1}; (iv) $E = 4\ 10^6$ Vm^{-1}. In (i) without and in (ii)–(iv) with hydrodynamic interactions.

strengths that were used in Figs. 1 and 4. The differences in configuration between the molecules in Fig. 6 are entirely due to the hydrodynamic interactions since we have not included any polarization effects, but the external field interacts with the fixed charges of the beads which is the same for every particle.

One way to qualitatively understand the origin of these configurational changes is to start from the following expression which gives the frictional force exerted on a particle j by the medium [36]

$$\mathcal{F}_j = -m\zeta(\dot{\boldsymbol{r}}_j - \boldsymbol{v}_j) \tag{8}$$

where m is the mass of the particle, ζ is the friction coefficient, $\boldsymbol{v}_j$ is the local velocity field at $\boldsymbol{r}_j$ due to the motion of all other particles except particle j. For a fluid at rest, this can be rewritten as [36]

$$\mathcal{F}_j = -\sum_k \boldsymbol{\Xi}_{jk} \cdot \dot{\boldsymbol{r}}_k \tag{9}$$

where $\boldsymbol{\Xi}$ is a friction tensor. This means of course that the frictional force exerted by the medium becomes more important as the particle velocity increases, but also that the magnitude and direction of this force will depend on the position of all other particles through the coupling matrix $\boldsymbol{\Xi}$, which is related to the diffusion tensor by $\mathbf{D}_{ij} = kT(\boldsymbol{\Xi}^{-1})_{ij}$. From the form of the diffusion tensor in eq. (1), it is also clear that those off-diagonal elements in **D** which correspond to a coupling between nearby lying particles will be larger than for those elements which represent interactions between particles separated by larger distances. With this simple picture in mind we can thus understand that there should be a deformation of the molecule due to varying forces on the subunits along the chain at high electric field strengths, when the particles move faster and when the relative importance of the randomizing Brownian motion is less, thus resulting e.g. in the differences shown in Fig. 6.

To make the relation between the value of S and μ and the chain configurations more transparent, we show in Fig. 7(a), S, and in 7(b), μ, as a function of time for two of the trajectories from which the snap-shots in Fig. 6 are taken, and we have also included the corresponding curves when polarization effects are taken into account. Looking first at Fig. 7(a) we see that the chains all start from a wholly prolate configuration, (since the chains lie along the x-axis), but become more and more oblate as time progresses. This process becomes faster when increasing the field strength, and for the highest field S goes through a minimum. This can be understood by looking at Fig. 8(a) which shows the configurations at four different times for curve (iii). When applying the field, the chain starts to bend and after 600 ns the configuration is only slightly prolate, almost in the form of a circular arc. After about 900 ns though, the chain becoms more U-shaped and is predominantly oblate after which the chain stretches somewhat making S increase slightly before a steady-state is reached. Looking at the dipole moment in Fig. 7(b), we can now understand that using this model, μ should increase as the molecule starts to bend when the electric field is applied. Since the bending of the chain

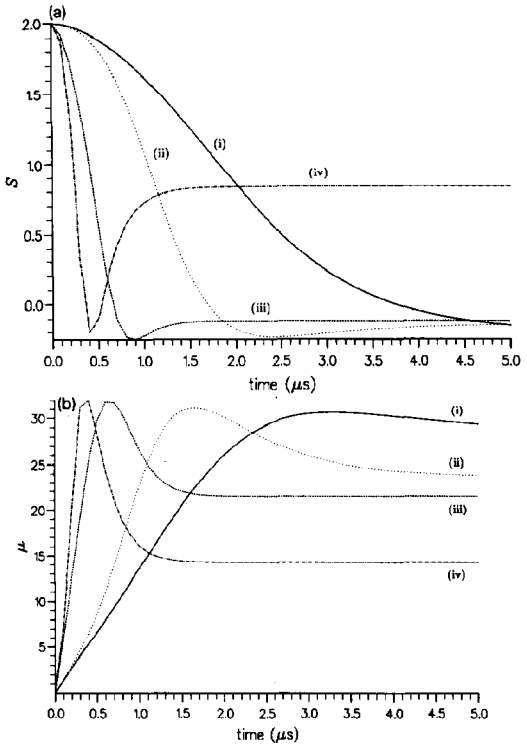

Fig. 7. (a) S as a function of time for trajectories generated as described in the text and in Fig. 6. For curves (i) and (ii) $E = 1\ 10^6\ \mathrm{Vm}^{-1}$, and for (iii) and (iv) $E = 4\ 10^6\ \mathrm{Vm}^{-1}$. Hydrodynamic interactions are included for all cases, while polarization effects are included for curves (ii) and (iv). (b) Dipole moment with respect to the centre of diffusion, (i)–(iv) having the same mening as in 7(a).

can be quite appreciable for the highest field strength, we can also predict that μ should go through a maximum, since, if one begins from a rod-like configuration and starts to bend the molecule in the shape of a circular arc, the dipole moment will first rise and go through a maximum at a bending angle of about 210° before it returns to zero for a circular shape.

Using the same model as above but including the polarization in the "moving-on" algorithm, still only using the coordinates of the subunits when calculating the dipole moment, gives the results shown in curves (ii) and (iv) in Figs. 7(a) and (b). In this case, the overall characteristics of the curves are much the same as for curves (i) and (iii), but when comparing e.g. curves (iii) and (iv), we can see that the steady-state value of S represents a considerably more prolate-like configuration than without polarization. The reason for this is shown in Fig. 8(b) which indicates the configurations at the same points in time as those of Fig. 8(a). The slight asymmetry seen for the different configurations in Fig. 8(b) is due to the fact that the redistributed charge is localized towards the centre of the subunits and not distributed continuously along the chain. It is seen that due to the local dipoles which are formed when the molecule starts to bend, the chain will obtain a narrow, more prolate U-shaped configuration. This can also be observed for the dipole moment, which shows quite a strong decrease after the maximum due to the more narrow configuration as compared to curve (iii). The results for curve (iv) can also be compared with starting from a fully stretched configuration going through a number of isosceles triangular configurations, ending up in two parallel strands which would give a configuration dependent dipole moment

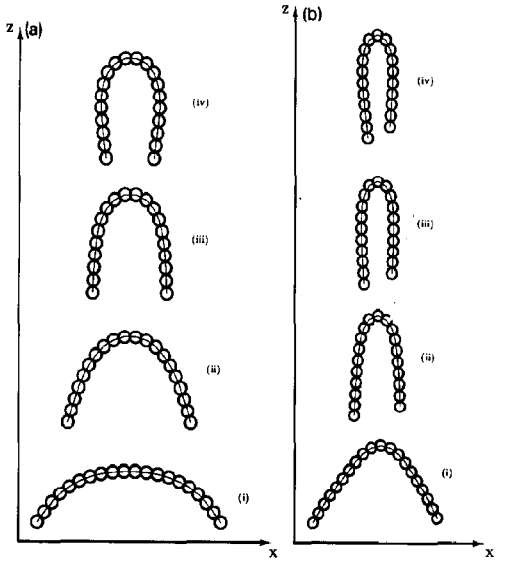

Fig. 8. (a) The configurations of the chains of curve (iii) in Fig. 7(a) and (b) shown at (i) 300 ns; (ii) 600 ns; (iii) 900 ns; and (iv) 1500 ns. (b) The configurations of the chains of curve (iv) in Figs. 7(a) and (b) shown at (i) 300 ns; (ii) 600 ns; (iii) 900 ns; and (iv) 1500 ns.

starting from zero, going through a maximum before returning to zero for the final structure.

The model calculations discussed above can now be used to interpret the results of the simulations presented in section 3. The decrease in the end-to-end distance and in S are thus due to the hydrodynamic interactions giving rise to a more or less bent structure and also inducing an orientation along the direction of the applied field, as shown in Fig. 5, curve (i). It is, however, important to stress that since the simulations are performed in three dimensions starting from random configurations and including the Brownian motion, the results of the two-dimensional model calculations, although important for a correct interpretation, are only qualitatively applicable when comparing with the simulations. This explains e.g. why the molecules in the simulations never become oblate (i.e. when $S < 0$), although both R_{ee} and μ show essentially the same features as in the model calculations (see e.g. curve (i) in Fig. 3(a) and curve (iii) in Fig. 7(b)). The results presented above also illustrate the importance of looking at several parameters when analyzing trajectories, for obtaining a more complete picture of what is going on, and why, during a simulation. In the present case, this is particularly true for the trajectories when polarization effects are included. Looking only at the end-to-end distance gives essentially the same picture as when only including the hydrodynamics. Examining S and μ, however, shows that also including the 'direct' orienting forces acting on the locally formed dipoles, makes the molecules keep a predominantly prolate shape during the orientation process, not going via the more rounded shapes resulting from a purely hydrodynamically induced orientation. Turning off the electric field while including polarization, however, results in the relaxation of these rather strained structures going through more open-like configurations, as indicated by the minimum in curve (iv) in Fig. 2(b).

The importance of performing several types of analyses is perhaps even more clear if one should only have looked at the orientation functions in Fig. 5. As was noticed in the previous section, curves (iii) and (iv) are qualitatively similar, although the structural difference between including hydrodynamics or not, is large. We can thus see that the orientation for curve (iii) is almost as large as for curve (iv) although the former represents a rather bent structure compared to the case when hydrodynamics is not included, when the chain orients like a stiff rod. The relatively high orientation obtained in the former case compared to curve (i) in Fig. 5 is then due to the local dipoles, each trying to orient in the direction of the applied field. A similar phenomenon can be seen in simulations of DNA gel electrophoresis where the end-to-end distance drops considerably after an initial maximum, but the orientation only decreases slightly [37,38]. (In that case, however, the orientation originates from the chain finding its way through a gel network.) We can further notice that the overshoot obtained for the curves including hydrodynamics, is also seen in electric birefringence experiments when increasing the field strength [3]. Another important feature of the orientation curves in Fig. 5 is that although the orientation, when including hydrodynamics and polarization effects, curve (iii), does not reach the same steady-state value as for a stiff chain forming a large dipole, curve (iv), the orientation is faster in the former case because its largest dimension decreases, thereby increasing its overall rotational motion.

Many of the steady-state configurations obtained during these simulations have shown rather large deviations from their equilibrium structure. It should, however, be kept in mind that the possibility of DNA forming local loops has been predicted in simulations [37,38] and observed in experiments of gel electrophoresis of DNA during orthogonal field alternating gel electrophoresis (OFAGE) using fluorescence microscopy [39], and is also seen in protein–DNA complexes like the nucleosome where the DNA winds around the histon octamer at about 80 base pairs per turn [6]. It is thus possible to introduce considerable strain to a DNA double helix without breaking its internal structure.

We can thus conclude that the interpretation of electric birefringence or electric dichroism experiments is a complex task and from the results presented above, it is suggested that some of the difficulties in interpreting such experiments

[3,4,16–22], can be due to not accounting for the possible contemporaneous change in configuration during the orientation process for a polyelectrolyte chain. This type of structural change would explain e.g. the increase in amplitude of the faster off-field relaxation mode of the two relaxation processes frequently observed [21], and also the inversion of the sign of the dichroism signal seen in some experiments [40]. Furthermore, these experimental observations are made at high electric field strengths, higher salt concentrations and for larger molecules, when the configurational changes discussed in the present paper should be increasingly important. More detailed calculations, however, are required for a quantitative assignment of how such structural changes affect both the on-field and off-field relaxation properties of polyelectrolyte molecules during electro-optical measurements. In future work, a more detailed model for the counterion polarization together with the hydrodynamic coupling between the ion atmosphere and the DNA should also be investigated.

Acknowledgements

This work was supported by the Swedish Natural Science Research Council. An allocation of computer time at the Supercomputer Centre North (SDCN) is also gratefully acknowledged.

References

1 Rotational dynamics of small and macromolecules, eds. Th. Dorfmüller and R. Pecora, Springer lecture notes in physics No. 293 (Springer, Berlin, 1987).
2 Dynamic properties of biomolecular assemblies, eds. S.E. Harding and A.J. Rowe, Special publication No. 74 (Royal Society of Chemistry, Cambridge, 1989).
3 R.J. Lewis, R. Pecora and D. Eden, Macromolecules 20 (1987) 2579.
4 S. Diekmann, W. Hillen, M. Jung, R.D. Wells and D. Pörschke, Biophys. Chem. 15 (1982) 157.
5 R. Pecora, Science, 251 (1991) 893.
6 A. Travers and A. Klug, Nature 327 (1987) 280.
7 T.J. Richmond, J.T. Finch, B. Rushton, D. Rhodes and A. Klug, Nature 311 (1984) 532.
8 M. Doi and S.F. Edwards, The Theory of Polymer Dynamics (Clarendon Press, Oxford, 1986).
9 S.R. Aragón and R. Pecora, Macromolecules 18 (1985) 1868.
10 D.L. Ermak and J.A. McCammon, J. Chem. Phys. 69 (1978) 1352.
11 S.A. Allison, Macromolecules 19 (1986) 118.
12 S.A. Allison, S.S. Sorlie and R. Pecora, Macromolecules 23 (1990) 1110.
13 E. Fredericq and C. Houssier, Electric dichroism and electric birefringence (Clarendon Press, Oxford, 1973).
14 E. Charney, Q. Rev. Biophys. 21 (1988) 1.
15 W.A. Wegener, R.M. Dowben and V.J. Koestner, J. Chem. Phys. 70 (1979) 622.
16 S. Diekmann, M. Jung and M. Teubner, J. Chem. Phys. 80 (1984) 1259.
17 D. Pörschke, Biopolymers 28 (1989) 1383.
18 D. Pörschke, J. Biomol. Struct. Dyn. 4 (1986) 373.
19 G.E. Plum and V.A. Bloomfield, Biopolymers 29 (1990) 1137.
20 R.J. Lewis, R. Pecora and D. Eden, Macromolecules 19 (1986) 134.
21 L. Song and J.M. Schurr, Biopolymers 30 (1990) 229.
22 R.J. Lewis, S.A. Allison, D. Eden and R. Pecora, J. Chem. Phys. 89 (1988) 2490.
23 E. Dickinson and C. Elvingson, J. Chem. Soc., Faraday Trans. II 84 (1988) 775.
24 J.A. Schellman, Biopolymers 13 (1974) 217.
25 P.J. Hagerman and B.H. Zimm, Biopolymers 20 (1981) 1481.
26 J. Rotne and S. Prager, J. Chem. Phys. 50 (1969) 4831.
27 G.D.J. Phillies, J. Chem. Phys. 81 (1984) 4046.
28 G. Dahlqvist and Å Björk, Numerical Methods (Prentice-Hall, Englewood Cliffs, NJ, 1974).
29 C. Elvingson, J. Comp. Chem. 12 (1991) 71.
30 M. Fixman, Macromolecules 19 (1986) 1204.
31 J.A. Aronovitz and D.R. Nelson, J. Phys. 47 (1986) 1445.
32 J.M. García Bernal and J. García de la Torre, Biopolymers 19 (1980) 751.
33 J. García de la Torre, A. Jiménez and J.J. Freire, Macromolecules 15 (1982) 148.
34 J. García de la Torre and V. Rodes, J. Chem. Phys. 79 (1983) 2454.
35 O. Kratky and G. Porod, Rec. Trav. Chim. Pays-Bas 68 (1949) 1106.
36 R. Zwanzig, Adv. Chem. Phys. 15 (1969) 325.
37 B. Nordén, C. Elvingson, M. Jonsson and B. Åkerman, in: Proc. of the 1st Int. Conf. on Electrophoresis, Supercomputing and the Human Genome, eds. C.R. Cantor and H.A. Lim (World Scientific, New York, NY, 1991) p. 173.
38 J.M. Deutsch, J. Chem. Phys. 90 (1989) 7436.
39 S. Gurrieri, E. Rizzarelli, D. Beach and C. Bustamante, Biochemistry 29 (1990) 3396.
40 J. Antosiewicz and D. Pörschke, Biophys. Chem. 33 (1989) 19.